PCCP

Low-Pressure and Nascent Yields of Stabilized Criegee Intermediates CH2OO and CH3CHOO in Ozonolysis of Propene

Journal:	*Physical Chemistry Chemical Physics*
Manuscript ID	CP-ART-06-2023-002590.R3
Article Type:	Paper
Date Submitted by the Author:	04-Sep-2023
Complete List of Authors:	Yang, Lei; University of California Riverside, Department of Chemistry Campos-Pineda, Mixtli; University of California Riverside, Department of Chemistry Hatem, Katia; University of California Riverside, Department of Chemistry Zhang, Jingsong; University of California Riverside, Department of Chemistry

Low-Pressure and Nascent Yields of Stabilized Criegee Intermediates CH_2OO and CH_3CHOO in Ozonolysis of Propene

Lei Yang, Mixtli Campos-Pineda,[§] Katia Hatem, and Jingsong Zhang[*]

Department of Chemistry

University of California, Riverside

Riverside, CA 92521

USA

[§] Present address: Centre for Research into Atmospheric Chemistry, University College Cork, T12 YN60, Ireland.

* Corresponding author. Email: jingsong.zhang@ucr.edu; Tel +1 951 827 4197; Fax: +1 951 827 4713. Also at Air Pollution Research Center, University of California, Riverside, California 92521, United States.

Keywords: ozonolysis, propene, Criegee intermediate, cavity ringdown spectroscopy

Abstract

The yields of stabilized Criegee intermediates (sCIs), both CH_2OO and CH_3CHOO, produced from ozonolysis of propene at low pressures (7-16 Torr) were measured indirectly using cavity ringdown spectroscopy (CRDS) and chemical titration with an excess amount of sulfur dioxide (SO_2). The method of monitoring the consumption of SO_2 as a scavenger and the production of secondary formaldehyde (HCHO) allows characterization of the total sCI and the stabilized CH_2OO yields at low pressure and in short residence time. Both the total sCI and the stabilized CH_2OO yields in the propene ozonolysis were found to decrease with decreasing pressure. By extrapolating the 7-16 Torr measurements to zero-pressure limit, the nascent yield of the total sCIs was determined to be 25 ± 2%. The ranges of nascent yields of stabilized CH_2OO and stabilized CH_3CHOO were estimated to be 20-25% and 0-5%, respectively. The branching ratios of the stabilized and high-energy CH_2OO^* and CH_3CHOO^* were also determined.

Introduction

As one of the major oxidation pathways of unsaturated volatile organic carbons (VOCs) in Earth's troposphere, ozonolysis plays an critical role in the formation of hydroxyl radical (OH) and the production of secondary organic aerosol (SOA).[1-4] The first step in the mechanism of ozonolysis involves the addition of ozone (O_3) to the olefinic bond of alkene, which produces a chemically activated five-membered ring called primary ozonide (POZ). POZ then undergoes a prompt decomposition, through cleavage of an O−O and a C−C bond, into a carbonyl compound and a carbonyl oxide known as Criegee intermediate (CI).[5] A small fraction of POZ may isomerize into ketohydroperoxide (KHP) and decompose into dialdehyde, OH radicals and other products.[6-9] With multiple resonance structures (zwitterion structures and biradical electronic configurations), CI has a rich reactivity and is the least stable among all its isomers.[10, 11] As ozonolysis reaction is highly exothermic, CIs are produced with broad internal energy distributions.[12] High-energy CIs

born with enough internal energy to surmount the isomerization or dissociation barriers can transform rapidly into dioxirane or vinyl hydroperoxide, and then decompose into OH radical, organic radicals, and other products on nanosecond timescales.[13] While stabilized Criegee intermediates (sCIs) are born with less energy, and have a longer lifetime to get involved in bimolecular reactions with atmospheric species or to undergo thermal decomposition.[14] The branching ratio of the high-energy CIs and sCIs depends both on the internal energy distributions and the heights of the dissociation or isomerization energy barriers of the CIs.

CIs have transient lifetimes in the troposphere because the rate coefficients for ozonolysis are small, while the unimolecular and bimolecular consumption reactions of CIs are rapid.[11] Owing to the low steady-state concentrations of CIs produced from ozonolysis, decades' efforts have proven the difficulty in detecting CIs directly in gas phase. In 2012, Welz and co-workers developed a new method to synthesize high-concentration sCIs in gas phase by using photolysis of diiodo-alkane in an excess amount of oxygen.[15] Since then, direct laboratory measurements on the unimolecular and bimolecular kinetics of sCIs have been reported.[16-22] However, the yields of the high-energy CIs and sCIs in ozonolysis of alkenes, which are related to the energy distributions of CIs and the branching ratio of various pathways in the reaction network of CIs, can only be measured in actual ozonolysis reactions. To measure the yield of sCIs in ozonolysis, chemical titration methods have been developed by using a scavenger to selectively and effectively react with all the sCIs produced from ozonolysis. Among the various molecules that have been studied and utilized as the sCI scavenger previously (such as hexafluoroacetone (HFA), formic acid (HCOOH), methanol (CH_3OH), formaldehyde (HCHO), water (H_2O) and carbon monoxide (CO)),[23, 24] sulfur dioxide (SO_2) is a commonly used scavenger in recent studies because of the characterizable spectral features of SO_2 or the end products (sulfuric acid (H_2SO_4)[25-28] or

carbonyls[29]) as well as the rapid reaction between SO_2 and sCIs (for example, IUPAC recommended k (SO_2 + CH_2OO) = 3.7×10^{-11} cm^3 $molecule^{-1}$ s^{-1}),[30] which allows SO_2 to capture all the sCIs before the thermal decomposition or other biomolecular reaction of sCIs. The total amount of sCIs is then determined by measuring either the amount of end products or the consumption of the scavenger ($\Delta[SO_2]$).[31-34]

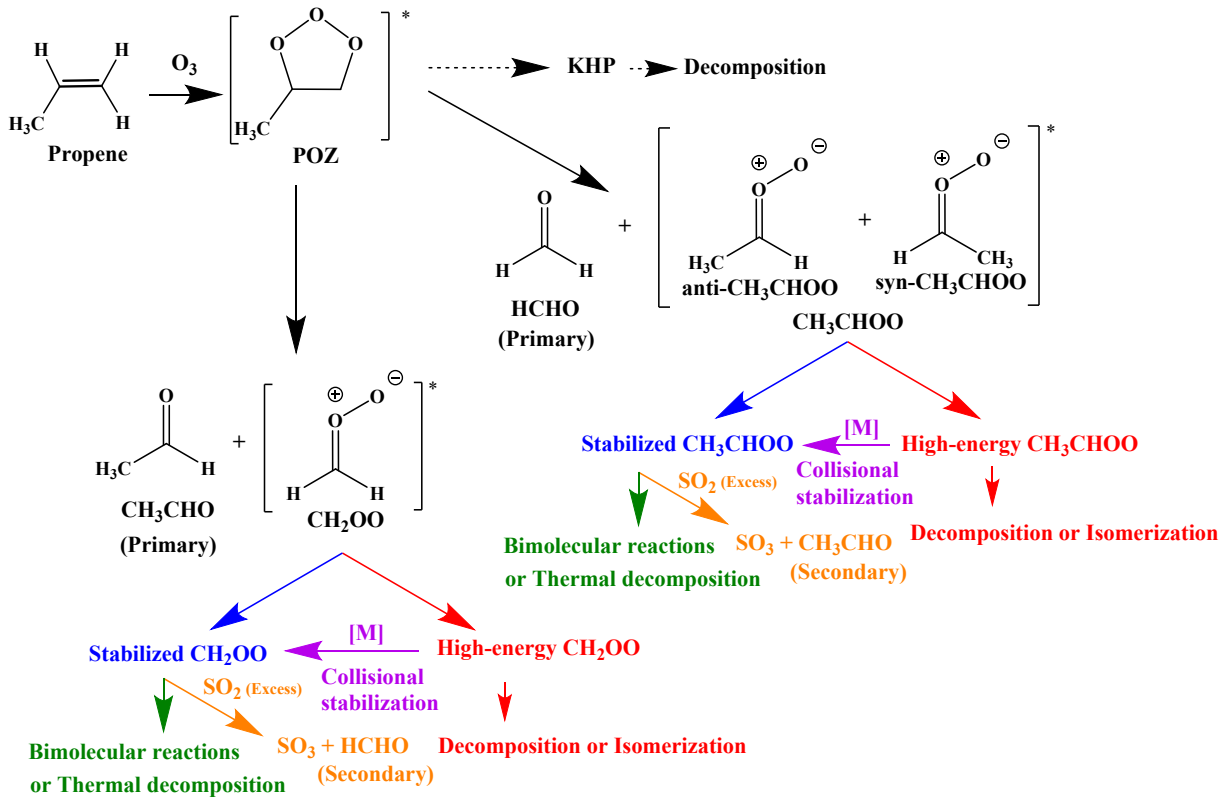

Scheme 1. Simplified reaction network of propene ozonolysis with an excess amount of SO_2 scavenger.

The production of sCIs can be from the direct dissociation of POZ, or from the collisional stabilization of the high-energy CIs. For example, as shown in the reaction network of propene ozonolysis in Scheme 1, the stabilized CH_2OO and CH_3CHOO come from the decomposition reaction of POZ (blue) as well as the thermalization of high-energy CH_2OO^* and CH_3CHOO^* after their deactivation collisions with other molecules (purple). As such, the yield of sCIs in ozonolysis of acyclic alkenes are dependent on pressure. Measuring the nascent yield of sCIs at zero-pressure limit is important for understanding the original energy profile of the ozonolysis of alkenes and the nascent energy distribution of CIs, which has attracted significant theoretical interest.[6, 35] However, even though the nascent yield of sCIs is an important benchmark for the reaction dynamics calculations and kinetics studies of CIs, most research on sCIs to date have focused on

the atmospheric-pressure region,[28, 29, 36] considering the difficulty and relatively larger uncertainty in determining sCI yields at low pressure. The sCI yields at the atmospheric pressure are attributed to a combination of factors, including the direct decomposition of POZ and the collisional stabilization of high-energy CIs. As a result, how the specific branching ratio of the different CIs evolve in this process remains a challenging topic.

In this work, we present a systematic study on the nascent and low-pressure yields of stabilized CH_2OO and CH_3CHOO produced from the ozonolysis of propene. Cavity ringdown spectroscopy (CRDS) in the near-UV region was used to quantify sCIs by monitoring the consumption of the added titrant SO_2 and the production of secondary HCHO. Spectral features of SO_2, O_3, and HCHO were fitted with their reference cross sections to obtain the number densities. The yields of sCIs in the ozonolysis of propene were measured at different low pressures from 7-16 Torr, and then the nascent yields of stabilized CH_2OO and CH_3CHOO were determined by extrapolation to the zero pressure. The branching ratio of the stabilized and high-energy CH_2OO^* and CH_3CHOO^* were also determined from the experiment.

Experimental methods

The average concentration of the targeted species was determined based on the following equation (1).

$$\alpha = \sum_i \sigma_i(\lambda) N_i + f(\lambda) = \frac{L}{c l_s}\left(\frac{1}{\tau} - \frac{1}{\tau_0}\right) \#(1)$$

which involves the following parameters: the absorption coefficient (α), the absorption cross-section of each species at different wavelengths ($\sigma_i(\lambda)$), the number density of each absorber (N_i), the distance between the two mirrors (L = 100 cm), the speed of light (c), the sample length (l_s =

57 cm), the ringdown time when absorber species are in the cavity (τ), the ringdown time in empty cavity (τ_0), and parameter $f(\lambda)$ which accounts for the unidentified broad extinction contribution at different wavelengths. As shown in Figure S1 in Electronic Supplementary Information (ESI), ozonolysis reactions were carried out in a cylindrical quartz flow cell with a sample length of 57 cm and diameter of 2.54 cm, which was used as a fast flow reactor. A mixture of propene and N_2 dilution gas was introduced into the reactor and combined with O_3 (~1% in O_2) generated by an ozone generator. In cases where the confirmation of sCI identity or sCI yield measurements were required, SO_2 (~4% in N_2) was mixed with propene prior to the introduction of O_3 to scavenge sCIs. To generate 10 Hz laser pulses in the range of 647-651 nm, a Lambda-Physik dye laser using DCM dye in methanol was pumped by a Continuum Surelite II Nd:YAG laser at 532 nm. The second harmonic was produced by an Inrad Autotracker Ⅲ in the range of 323.5-325.5 nm. A pair of highly reflective mirrors centered at 330 nm (>99.9%, Layertec GmbH) was used to establish a baseline ringdown time (τ_0) of approximately 5 μs. With the long effective optical path and high sensitivity ($\alpha_{min} \sim 3\times10^{-8}$ cm^{-1}), CRDS was capable of measuring signals from low-concentration species. The flow parameters of the reactor are listed in Table S1 in ESI, which shows that the radial diffusion in the flow cell can be ignored under our experimental conditions and the flow reactor can be reasonably modelled as a plug flow reactor (PFR) using the Kintecus software package[37].

As shown in Figure 1 and Figure S2, the UV spectra (black lines) of the ozonolysis reaction (propene + O_3) at 323.5-325.2 nm were analyzed by fitting the spectral features of O_3 and HCHO (red lines) to determine the final concentration of O_3 ($[O_3]_f$) and the initial concentration of primary HCHO ($[HCHO]_i$). While in the titration reaction (propene + O_3 + SO_2), the spectral signatures of O_3, HCHO, and SO_2 can also be isolated from some broad background contributions of secondary

reactions (Figure 1 and Figure S3), enabling the determination of the final concentrations of SO_2

and HCHO ($[SO_2]_f$ and $[HCHO]_f$ (from both primary and secondary HCHO), and the O_3

concentration ($[O_3]_f$) remained unchanged with or without SO_2). The initial O_3 and SO_2

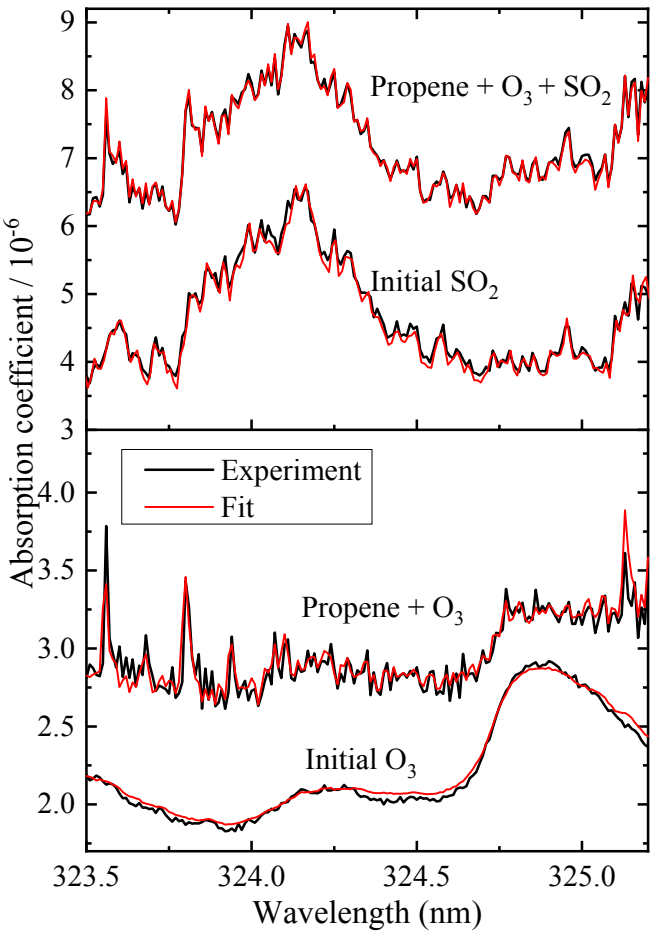

Figure 1. Representative near-UV CRDS spectra (black) in ozonolysis of propene (propene + O_3) and the titration reaction with SO_2 (propene + O_3 + SO_2), along with the fitted spectra using the corresponding reference cross sections (red). Concentrations of the reactants and products in this example (unit: molecules cm^{-3}): $[O_3]_i = 1.59 \times 10^{14}$, $[propene]_i = 9.97 \times 10^{16}$, $[O_3]_f = 9.00 \times 10^{13}$, $[SO_2]_i = 3.66 \times 10^{14}$, $[SO_2]_f = 3.45 \times 10^{14}$, $[HCHO]_i$ (the sharp features in propene + O_3) $= 4.2 \times 10^{13}$, $[HCHO]_f$ (in propene + O_3 + SO_2) $= 5.7 \times 10^{13}$. The total pressure was 10 Torr. The residence time inside the flow reactor was 0.92 s. All experiments were carried out at room temperature.

concentrations ($[O_3]_i$ and $[SO_2]_i$) were measured by using nitrogen (N_2) to replace the corresponding reactants (alkene or O_3) under the same flow conditions. To ensure the accuracy of the measurement, reference cross sections of O_3, SO_2, and HCHO were carefully selected from the MPI Mainz UV/vis Spectral Atlas[38] based on the appropriate wavelength ranges and spectral

resolution. These reference cross sections were then fitted to our experimental spectra, allowing for the creation of custom references that effectively minimized any differences in measurement sensitivities. This approach was particularly important for HCHO, as its rovibronic features could be influenced by various energy distributions during ozonolysis reaction and potentially shifted in the experimental spectra.

As the reaction rate coefficient k (OH + propene) ranges from 2.5-2.9×10^{-11} cm^3 $molecule^{-1}$ s^{-1} at 7-760 Torr and 298K, the large excess amount of propene present in the reaction mixture (approximately 1.0×10^{17} molecules cm^{-3}) can rapidly react with the OH radicals produced by ozonolysis and completely deplete them. In the meantime, sCIs were scavenged by SO_2 with fast reaction rate coefficients, for example, k (CH_2OO + SO_2) = 3.7×10^{-11} cm^3 $molecule^{-1}$ s^{-1}, k (*syn*-CH_3CHOO + SO_2) = 2.6×10^{-11} cm^3 $molecule^{-1}$ s^{-1} and k (*anti*-CH_3CHOO + SO_2) = 1.4×10^{-10} cm^3 $molecule^{-1}$ s^{-1}. When the amount of SO_2 present in the reaction mixture was in a large excess of the total amount of sCIs (for example, in this work $[SO_2]_i$ ~3.5×10^{14} molecules cm^{-3}), all sCIs produced in ozonolysis can be captured by SO_2, and the amount of consumed SO_2 was equal to the amount of sCIs. Therefore, the total yield of sCIs can be determined by the following equation (2).

$$\text{Yield of sCI} = \frac{\Delta[SO_2]}{\Delta[O_3]} \#(2)$$

where the amount of consumed SO_2 is $\Delta[SO_2] = [SO_2]_i - [SO_2]_f$ and the amount of consumed O_3 is $\Delta[O_3] = [O_3]_i - [O_3]_f$.

At the same time, HCHO and SO_3 were produced in the reaction between CH_2OO and SO_2 as the major pathway, while the reaction between CH_3CHOO and SO_2 produced CH_3CHO and SO_3 after the decomposition of the chemically-activated secondary ozonide (SOZ) at low pressure.[21,

[39-41] The amount of secondary HCHO produced after adding SO_2, $\Delta[HCHO] = [HCHO]_f - [HCHO]_i$, is thus related to the amount of stabilized CH_2OO. Therefore, the yield of stabilized CH_2OO can be determined by the following equation (3), and the yield of stabilized CH_3CHOO is equal to the difference of the total yield of sCIs and the yield of stabilized CH_2OO. Since bimolecular reactions of CH_2OO might also produce HCHO before SO_2 was added, the $\Delta[HCHO]/\Delta[O_3]$ measured with this method should be considered as a lower limit of the stabilized CH_2OO yield.

$$\text{Yield of stabilized } CH_2OO \geq \frac{\Delta[HCHO]}{\Delta[O_3]} \#(3)$$

As shown in Scheme 1, the production of the total amount of CH_2OO and CH_3CHOO intermediates from initial decomposition of POZ in propene ozonolysis are equal to that of the corresponding primary carbonyl products, CH_3CHO and HCHO, respectively. Thus, the total yield of CH_3CHOO (including *syn*/*anti*-conformers in the full internal energy profile) is equal to the yield of the primary HCHO, and can be determined by calculating the ratio of the amount of HCHO produced in ozonolysis ($[HCHO]_i$) and the consumed O_3 ($\Delta[O_3]$), as shown in equation (4). Note that in propene ozonolysis at the atmospheric pressure, the total yields of carbonyls were measured to be in the range of 100% to 110%,[36, 42] with CH_2OO, CH_3CHOO, or KHP possibly producing a small amount of secondary HCHO; thus in this system, the measured $[HCHO]_i$ should be considered as the upper limit for the primary HCHO. Our kinetic model estimates the extent of this overestimation, as discussed in ESI (see Table S2-S5).

$$\text{Yield of } CH_3CHOO \leq \frac{[HCHO]_i}{\Delta[O_3]} \#(4)$$

Theoretical calculations showed that 12% of POZ produced in ethene ozonolysis can isomerize into KHP,[6] yet there is no reported study on propene ozonolysis to date. Assuming the KHP

branching in propene ozonolysis also up to 12%, the total yield of CH_2OO (including both stabilized CH_2OO and high-energy CH_2OO^*) can be obtained by subtracting the yield of primary HCHO (the total yield of CH_3CHOO) from the total CI yield of 88-100%. Thus, using the equations listed above and the relationships indicated in Scheme 1, the yields of stabilized CH_2OO, high-energy CH_2OO^*, stabilized CH_3CHOO, and high-energy CH_3CHOO^* can all be obtained using the near-UV CRDS and the SO_2 titration method.

Equation 2 is valid when the concentration of SO_2 is high enough to completely react with/scavenge all the sCIs produced from the ozonolysis reaction, before the sCIs can undergo any further unimolecular or bimolecular reactions with other species such as the O_3, alkene, or HCHO in the system. However, it should be noted that using too much SO_2 may also cause saturation of the absorption spectra and limit the accuracy of the measurements. This is because CRDS has a limited dynamic range in measurement, typically 2 orders of magnitude. Therefore, exceeding the upper limit of the dynamic range would result in a rapid increase of the ringdown decay rate, leading to signal saturation and noisy measurements. To avoid using an excessively high concentration of SO_2, which could also lead to the formation of secondary products and an increase in the broad background in the absorption spectra, a titration curve was measured as shown in Figure 2, which allowed for the determination of the minimum amount of SO_2 required to completely consume all the sCIs. The titration curve was obtained by measuring the change in the ratio of consumed SO_2 to consumed O_3 ($\Delta[SO_2]/\Delta[O_3]$) as the initial concentration of SO_2 was varied under identical conditions of pressure, residence time, and initial propene and O_3 concentrations. This approach ensured that the optimal amount of SO_2 was used to titrate the sCIs while avoiding any unnecessary excess. Since O_3 was the limiting reagent in the ozonolysis reaction studied in this experiment (with the propene concentration being approximately three

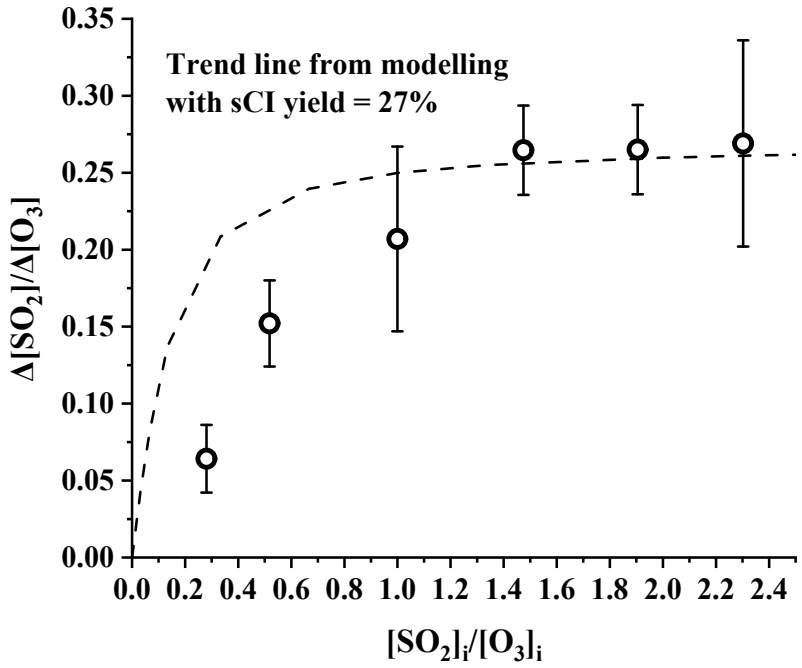

Figure 2. The titration curve showing the variation in the consumption of SO_2 in propene ozonolysis as the initial SO_2 concentration was varied at a total pressure of 10 Torr. The horizontal axis represents the ratio of the initial SO_2 concentration to the initial O_3 concentration, which reflects the excess extent of the SO_2 titrant. The initial O_3 concentration was kept constant at approximately 1.5×10^{14} molecules cm^{-3} throughout the titration curve. The vertical axis is the ratio of the consumed amounts of SO_2 and O_3. The curve reached a maximum of approximately 27% when concentration of the added SO_2 was high enough to fully titrate all the sCIs produced during propene ozonolysis. The trend line was calculated using kinetic modelling. Error bars represent one standard deviation in repeated measurements at each SO_2 concentration.

orders of magnitude higher than the O_3 concentration), the ratio of the initial concentrations of SO_2 and O_3 was plotted on the horizontal axis. As the initial SO_2 concentration increased, the ratio of $\Delta[SO_2]/\Delta[O_3]$ increased and eventually levelled off. At this plateau, $\Delta[SO_2]/\Delta[O_3]$ approached a constant value, indicating the maximum consumption of SO_2 and completion of the titration of sCIs. This plateau was observed at an initial $[SO_2]/[O_3]$ ratio higher than 1.5, corresponding to SO_2 concentration higher than 2.3×10^{14} molecules cm^{-3}. Based on the consumed O_3 being about 40-

50% of its initial concentration and the typical yield of sCIs in ozonolysis being less than 40%, the amount of SO_2 needed to reach the plateau in the titration curve was more than 10 times higher than the total amount of sCIs produced in ozonolysis. In the sCI measurement experiments under different pressures, high initial concentrations of SO_2 were used with the $[SO_2]/[O_3]$ ratio being approximately 2.3. This allowed for the efficient scavenging of sCIs via the SO_2 + sCI reactions, which have a large rate constant (e.g., k (SO_2 + CH_2OO) = 3.7×10^{-11} cm^3 $molecule^{-1}$ s^{-1}) and ensured that the SO_2 + sCI scavenging reaction was the dominant pathway for the sCI removal, outcompeting all other reaction pathways of sCI. The titration curve was further supported by the results of kinetic modelling built for the titration reaction using the Kintecus software package,[37] as presented in Table S2 in ESI. The trend line of $\Delta[SO_2]/\Delta[O_3]$ calculated from the kinetic modelling (dashed line in Figure 2) was found to be in good agreement with our experimental measurements, except for the initial part of the titration curve where the SO_2 concentration was not high enough to dominate over other reaction pathways involving CH_2OO and CH_3CHOO. In the initial rising part of the curve where all reaction pathways of CH_2OO compete and are involved, the reaction kinetics is complex and harder to model accurately; whereas it becomes easier to model the plateau where SO_2 is sufficient to dominate other pathways and the kinetics becomes "simple". While the initial gap indicates that there is room to improve our kinetic model, the agreement between the kinetic model and experimental results in the plateau region helps validate the endpoint of titration (the main focus of this work). The experimental measurements on $\Delta[SO_2]/\Delta[O_3]$ in this study were subject to noticeable error bars, representing one standard deviation of repeated measurements. The extent of the reactions in the short residence time (approximately 0.9 s) was limited by the relatively slow reaction between propene and O_3 (k (propene + O_3) = 1.05×10^{-17} cm^3 $molecule^{-1}$ s^{-1}). Despite the relatively large error bars, it was

crucial to maintain a short residence time of less than 1 second to prevent accumulation of secondary products such as formic acids, carbonyls, and SOA. These byproducts can not only contribute to a broad UV absorption background and decrease detection sensitivity but also compete with SO_2 in the reaction with sCIs, as observed in our experiments and confirmed by kinetic modelling calculations.

Results and discussion

As propene is an asymmetric alkene, its ozonolysis produces formaldehyde oxide (CH_2OO) and *syn*/*anti* conformers of acetaldehyde oxide (*syn*/*anti*-CH_3CHOO). Figure 3 shows the total yield of sCIs and the yield of stabilized CH_2OO produced from ozonolysis of propene in the pressure range of 7-16 Torr. The initial $[SO_2]_i/[O_3]_i$ ratio was kept at 2.3-2.5 to ensure that sCIs can be scavenged completely at all the pressures. The linear fit of the trend shows that the total sCI yield decreases slightly from 28% to 26% when the pressure decreases from 16 to 7 Torr. The nascent yield of total sCIs in propene ozonolysis is determined to be 25 ± 2% after extrapolation to the zero-pressure limit. The yield of secondary HCHO after adding SO_2 (the lower limit of the stabilized CH_2OO) also showed a small decrease with decreasing pressure in the 7-16 Torr region, and the lower limit of the nascent yield of stabilized CH_2OO is 20 ± 2% at zero pressure. The uncertainty of the nascent yields was estimated from the standard error of the weighted linear fit using the least-squares method and corrected with the critical value in 95% confidence *t*-test (more details in the description of Table S6 and Table S7 in ESI). The yield of HCHO in ozonolysis of propene was measured to be 62 ± 5%, which contains both primary HCHO yield and small secondary HCHO yield produced from other pathways. According to our kinetic modelling, the

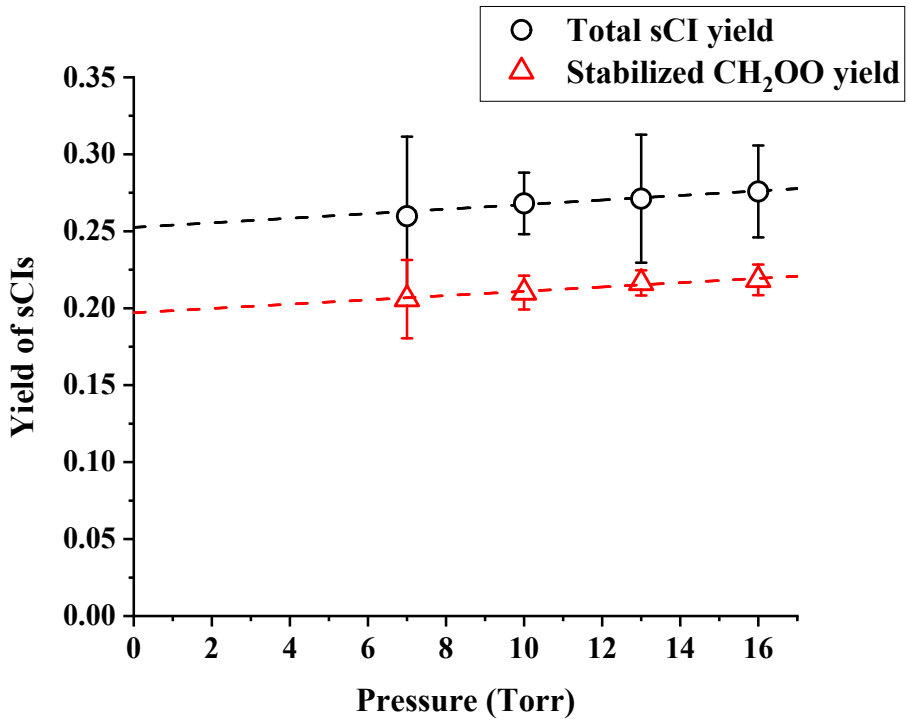

Figure 3. Low-pressure yield of sCIs (stabilized CH_2OO and CH_3CHOO) produced in ozonolysis of propene measured below 16 Torr. Total sCI yield (black) was determined from the consumption of SO_2, while the yield of stabilized CH_2OO (red) was calculated from the production of secondary HCHO after adding SO_2. The dashed lines represent the weighted linear fit of the experimental data points and are extrapolated to the zero-pressure limit. Error bars represent one standard deviation in repeated measurements at each pressure.

yield of secondary HCHO produced from the CH_2OO bimolecular reactions is ≤ 5% and there could be ~3% additional HCHO from the KHP decomposition (see Table S3). Thus, the total yield of *syn*/*anti* conformers of CH_3CHOO determined from the primary yield of HCHO from equation (4) is estimated to be in a range of 54-62%, and the total yield of CH_2OO is 29-43% (assuming 0-12% of KHP yield from the POZ decomposition).[6] From these results, the nascent yields of stabilized CH_2OO and stabilized CH_3CHOO are calculated to be 20-25% and 0-5%, while the nascent yield of the high-energy CH_2OO^* and high-energy CH_3CHOO^* are 9-18% and 53-57%, respectively. The specific values of the CI yields under different assumptions are listed in Table S3.

The yield of HCHO in ozonolysis reported here, 62 ± 5%, is consistent with the previous studies of 60-65% yield at the atmospheric pressure,[29, 36, 42-44] which indicates that pressure may not have a large impact on the branching ratio of the total CH_2OO and CH_3CHOO produced from decomposition of POZ in propene ozonolysis. However, the energy distribution of CIs and the total sCI yield are dependent on the pressure. In the previous studies at the atmospheric pressure, the total yield of sCIs in propene ozonolysis has been determined to be 44%, 25 ± 2% and 34 ± 1% by Horie et al.,[36] Hatakeyama et al.[28] and Newland et al,[29] respectively. Among these studies, Hatakeyama et al.[28] and Newland et al.[29] used SO_2 as the scavenger and qualified either the associated product H_2SO_4 or the consumed SO_2, respectively, while Horie et al.[36] added HCHO as the scavenger and measured the adduct between sCIs and HCHO. Our experimental value of the total nascent sCI yield at the zero pressure, 25 ± 2%, is about 9% lower than the 34 ± 1 % atmospheric sCI yield in propene ozonolysis reported by Newland et al.[29], who used the same scavenger and quantification method ($\Delta[SO_2]$ for total sCIs) with this work. Newland et al.[29] also reported the yield of stabilized CH_2OO in propene ozonolysis being 23% at the atmospheric pressure, measured from the increase of secondary HCHO after adding SO_2 as in the current work. The nascent yield of stabilized CH_2OO measured in this work is about 3% lower than the atmospheric yield, yet both of them should be considered as lower limits because secondary HCHO were already produced from bimolecular reactions of CH_2OO prior to adding SO_2.

From the ratio between the nascent yield of stabilized CH_2OO (20-25%) and the total yield of CH_2OO (29-43%), the nascent stabilization factor of CH_2OO is determined to be 52-74%. The specific values of the CI stabilization factors under different assumptions are listed in Table S3. Newland et al.[29] reported the stabilization factor of CH_2OO to be 60% at atmospheric pressure, calculated from the ratio between the lower limit of stabilized CH_2OO yield (23%) and the initial

CH_3CHO yield of 38%. Thus, if taking the same method, the nascent stabilization factor of CH_2OO at low pressure in this work is ~8% lower than that at atmospheric pressure. Similarly, the nascent stabilization factor of CH_3CHOO can be estimated to be 0-9% at the zero pressure limit, and it is about 9-30% lower than that at the atmospheric pressure.[29] This observation agrees with the relatively low nascent yield of stabilized CH_3CHOO of 0-5% measured in ozonolysis of *trans*-2-butene and *cis*-2-butene.[32, 33] Compared to CH_3CHOO, CH_2OO has a much higher stabilization factor because of its high isomerization barriers to form dioxirane and hydroperoxide (reported to be 18.2−19.1 and 30.8−31.8 kcal/mol, respectively),[12, 35] while the *syn*-conformers of the larger sCIs can undergo a lower barrier pathway through the 1,4-hydrogen migration to form alkenyl hydroperoxide, and this process is enhanced by tunnelling (barrier of *syn*-CH_3CHOO to form vinyl hydroperoxide is 17.05 kcal/mol).[11, 12, 45]

Compared to the 20% nascent yield of sCIs in ethene ozonolysis,[34] the total nascent sCI yield in propene ozonolysis is about 5% higher. Although the nascent stabilized CH_2OO yield is about the same in propene and ethene ozonolysis (~ 20%), considering that the branching ratio of the CH_2OO pathway from POZ is only ~29-43% in propene ozonolysis (while it is 88-100% in ethene ozonolysis), the nascent stabilization factor of CH_2OO is 29-54% higher in propene ozonolysis compared to that in ethene ozonolysis. Assuming the internal energy is distributed evenly on POZ, after the cleavage of POZ, energy taken away by the carbonyl coproduct would increase with the increase of its size. The acetaldehyde (CH_3CHO) coproduct of CH_2OO in propene ozonolysis can take away more internal energy than the HCHO coproduct of CH_2OO in ethene ozonolysis, and thus the mean internal energy of CH_2OO in propene ozonolysis is lower than that in ethene ozonolysis.

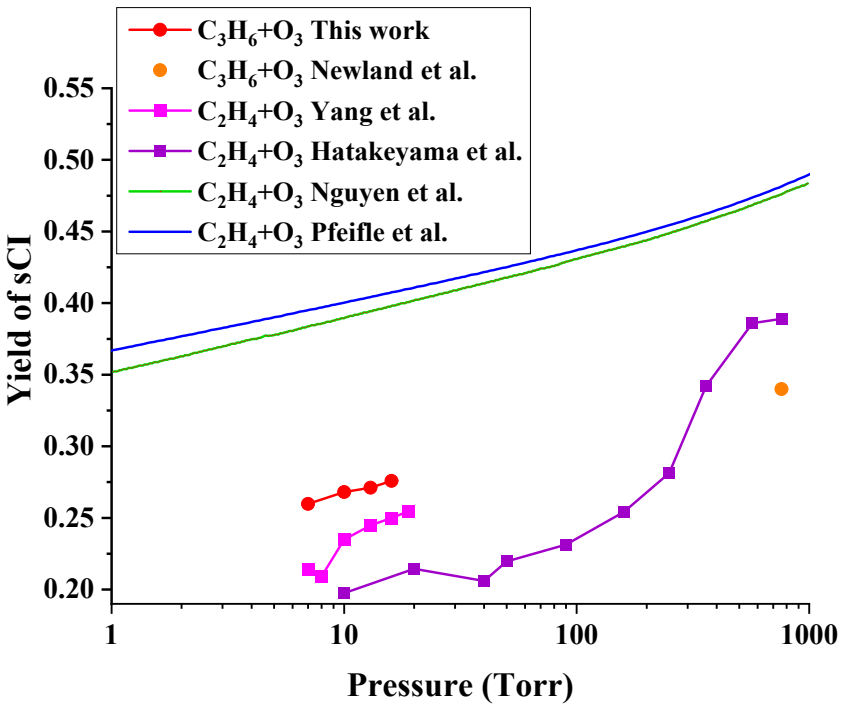

Figure 4. The total sCI yield in propene ozonolysis measured by experimental works compared to the sCI yields reported by experimental and theoretical works for the ethene ozonolysis.[6, 25, 29, 34, 35]

Previous theoretical calculations suggest that the collisional stabilization of POZ in ozonolysis of alkene is negligible,[35] and that the pressure-dependent behavior of sCI yields is due to collisional stabilization of high-energy CIs with buffer gases. In Figure 4, the low-pressure sCI yields measured by this work is compared to the sCI yields measured by Newland et al.[29] at atmospheric pressure and the increasing trend of sCI yields reported by experimental and theoretical works for ethene ozonolysis at 1-1000 Torr.[6, 25, 34, 35] Although the alkenes are different, the general trends are similar to those by theoretical predictions with respect to the logarithmic pressure.[6, 35] The sCI yields calculated by Nguyen et al.[35] were based on statistical energy partitioning, while those by Pfeifle et al.[6] were from trajectory models (non-statistical theories). A few other theoretical works on ozonolysis support the nonergodic and nonstatistical behaviors of energy partitioning in the

ozonolysis reactions of propene and vinyl ethers.[46, 47] Compared to the previous experimental studies on ethene ozonolysis,[25, 34] the increase of sCI yield is smaller in propene ozonolysis at 7-760 Torr, which might suggest a smaller collisional stabilization effect of CH_3CHOO than CH_2OO. By comparing the predictions from the theoretical models with the experimental results, future researchers can assess the accuracy and reliability of their models and potentially refine them to better describe the behavior of CIs.

Conclusions

The yields of the total sCIs, the stabilized CH_2OO, and the stabilized CH_3CHOO produced in ozonolysis of propene were determined at low pressures from 7 to 16 Torr by monitoring the consumption of SO_2 scavenger as well as the production of secondary HCHO using the near-UV CRDS. Nascent yields of these sCIs were obtained from extrapolation to the zero-pressure limit, and the branching ratio of the stabilized and high-energy CH_2OO^* and CH_3CHOO^* were also determined. CH_2OO has a higher nascent stabilization factor than CH_3CHOO due to its relatively higher energy barrier for isomerization and dissociation. The nascent stabilization factor of CH_2OO is higher in propene ozonolysis than in ethene ozonolysis, because the larger size of the carbonyl co-product in propene ozonolysis can take away more energy. The branching ratio obtained from the current study can be used as benchmarks for future theoretical calculations.

Electronic Supplementary Information (ESI)

The Supplementary Information is available free of charge. The Supplementary Information provides more experimental and modelling details. Figures S1−S4 present the experimental setup,

the broad absorption background $f(\lambda)$ in the spectra, and the comparison between modelling and experimental sCI yields in propene ozonolysis. Tables S1−S8 list flow parameters of the reactor, kinetic modelling, summarized nascent CI/carbonyl yields based on different assumptions, and sCI yields measurements at each pressure.

Conflicts of Interest

There are no conflicts of interest to declare.

Acknowledgements

This work was supported by the U.S. National Science Foundation (CHE-2155232). L. Yang acknowledges the support from a UC Riverside Dissertation Research Grant. M. Campos-Pineda acknowledges the support from a UCMEXUS-CONTACYT Doctoral Fellowship.

Notes and references

1. S. E. Paulson and J. J. Orlando, *Geophys. Res. Lett.*, 1996, **23**, 3727-3730.
2. B. J. Finlayson-Pitts and J. N. Pitts, *Chemistry of the Upper and Lower Atmosphere: Theory, Experiments, and Applications*, Academic Press, San Diego, 2000.
3. R. Atkinson and J. Arey, *Chem. Rev.*, 2003, **103**, 4605-4638.
4. J. H. Kroll and J. H. Seinfeld, *Atmos. Environ.*, 2008, **42**, 3593-3624.
5. R. Criegee, *Angew. Chem., Int. Ed. Engl.*, 1975, **14**, 745-752.

6. M. Pfeifle, Y. T. Ma, A. W. Jasper, L. B. Harding, W. L. Hase and S. J. Klippenstein, *J. Chem. Phys.*, 2018, **148**, 174306.

7. A. C. Rousso, N. Hansen, A. W. Jasper and Y. Ju, *J. Phys. Chem. A*, 2018, **122**, 8674-8685.

8. N. Genossar, J. P. Porterfield and J. H. Baraban, *Phys. Chem. Chem. Phys.*, 2020, **22**, 16949-16955.

9. C. S. Lewin, O. Herbinet, G. A. Garcia, P. Arnoux, L.-S. Tran, G. Vanhove, L. Nahon, F. Battin-Leclerc and J. Bourgalais, *Chem. Commun.*, 2022, **58**, 13139-13142.

10. C. A. Taatjes, *Annu. Rev. Phys. Chem.*, 2017, **68**, 183-207.

11. D. L. Osborn and C. A. Taatjes, *Int. Rev. Phys. Chem.*, 2015, **34**, 309-360.

12. M. Olzmann, E. Kraka, D. Cremer, R. Gutbrod and S. Andersson, *J. Phys. Chem. A*, 1997, **101**, 9421-9429.

13. G. T. Drozd, T. Kurtén, N. M. Donahue and M. I. Lester, *J. Phys. Chem. A*, 2017, **121**, 6036-6045.

14. J. Jr-Min Lin and W. Chao, *Chem. Soc. Rev.*, 2017, **46**, 7483-7497.

15. O. Welz, J. D. Savee, D. L. Osborn, S. S. Vasu, C. J. Percival, D. E. Shallcross and C. A. Taatjes, *Science*, 2012, **335**, 204-207.

16. J. D. Fenske, A. S. Hasson, A. W. Ho and S. E. Paulson, *J. Phys. Chem. A*, 2000, **104**, 9921-9932.

17. O. Welz, A. J. Eskola, L. Sheps, B. Rotavera, J. D. Savee, A. M. Scheer, D. L. Osborn, D. Lowe, A. Murray Booth, P. Xiao, M. Anwar H. Khan, C. J. Percival, D. E. Shallcross and C. A. Taatjes, *Angew. Chem., Int. Ed.*, 2014, **53**, 4547-4550.

18. F. Liu, J. M. Beames, A. S. Petit, A. B. McCoy and M. I. Lester, *Science*, 2014, **345**, 1596-1598.

19. Y. Liu, K. D. Bayes and S. P. Sander, *J. Phys. Chem. A*, 2014, **118**, 741-747.

20. Y.-P. Lee, *J. Chem. Phys.*, 2015, **143**, 020901.

21. C. A. Taatjes, O. Welz, A. J. Eskola, J. D. Savee, A. M. Scheer, D. E. Shallcross, B. Rotavera, E. P. F. Lee, J. M. Dyke, D. K. W. Mok, D. L. Osborn and C. J. Percival, *Science*, 2013, **340**, 177-180.

22. L. Sheps, *J. Phys. Chem. Lett.*, 2013, **4**, 4201-4205.

23. G. T. Drozd and N. M. Donahue, *J. Phys. Chem. A*, 2011, **115**, 4381-4387.

24. G. T. Drozd, J. Kroll and N. M. Donahue, *J. Phys. Chem. A*, 2011, **115**, 161-166.

25. S. Hatakeyama, H. Kobayashi, Z. Y. Lin, H. Takagi and H. Akimoto, *J. Phys. Chem.*, 1986, **90**, 4131-4135.

26. J. P. Hakala and N. M. Donahue, *J. Phys. Chem. A*, 2016, **120**, 2173-2178.

27. T. Berndt, R. Kaethner, J. Voigtländer, F. Stratmann, M. Pfeifle, P. Reichle, M. Sipilä, M. Kulmala and M. Olzmann, *Phys. Chem. Chem. Phys.*, 2015, **17**, 19862-19873.

28. S. Hatakeyama, H. Kobayashi and H. Akimoto, *J. Phys. Chem.*, 1984, **88**, 4736-4739.

29. M. J. Newland, B. S. Nelson, A. Munoz, M. Rodenas, T. Vera, J. Tarrega and A. R. Rickard, *Phys. Chem. Chem. Phys.*, 2020, **22**, 13698-13706.

30. R. A. Cox, M. Ammann, J. N. Crowley, H. Herrmann, M. E. Jenkin, V. F. McNeill, A. Mellouki, J. Troe and T. J. Wallington, *Atmos. Chem. Phys.*, 2020, **20**, 13497-13519.

31. M. J. Newland, A. R. Rickard, L. Vereecken, A. Muñoz, M. Ródenas and W. J. Bloss, *Atmos. Chem. Phys.*, 2015, **15**, 9521-9536.

32. M. Campos-Pineda and J. Zhang, *Sci. China Chem.*, 2018, **61**, 850–856.

33. M. Campos-Pineda and J. Zhang, *Chem. Phys. Lett.*, 2017, **683**, 647-652.

34. L. Yang, M. Campos-Pineda and J. Zhang, *J. Phys. Chem. Lett.*, 2022, **13**, 11496-11502.

35. T. L. Nguyen, H. Lee, D. A. Matthews, M. C. McCarthy and J. F. Stanton, *J. Phys. Chem. A*, 2015, **119**, 5524-5533.

36. O. Horie and G. K. Moortgat, *Atmos. Environ.*, 1991, **25**, 1881-1896.

37. J. C. Ianni, in *Computational Fluid and Solid Mechanics 2003*, ed. K. J. Bathe, Elsevier Science Ltd., Oxford, 2003, pp. 1368-1372.

38. H. Keller-Rudek, G. K. Moortgat, R. Sander and R. Sorensen, *Earth Syst. Sci. Data*, 2013, **5**, 365-373.

39. Y. Y. Wang, M. R. Dash, C. Y. Chung and Y. P. Lee, *J. Chem. Phys.*, 2018, **148**, 064301.

40. L. Vereecken, H. Harder and A. Novelli, *Phys. Chem. Chem. Phys.*, 2012, **14**, 14682-14695.

41. K. T. Kuwata, E. J. Guinn, M. R. Hermes, J. A. Fernandez, J. M. Mathison and K. Huang, *J. Phys. Chem. A*, 2015, **119**, 10316-10335.

42. E. C. Tuazon, S. M. Aschmann, J. Arey and R. Atkinson, *Environ. Sci. Technol.*, 1997, **31**, 3004-3009.

43. E. Grosjean, J. B. de Andrade and D. Grosjean, *Environ. Sci. Technol.*, 1996, **30**, 975-983.

44. A. R. Rickard, D. Johnson, C. D. McGill and G. Marston, *J. Phys. Chem. A*, 1999, **103**, 7656-7664.

45. T. A. Stephenson and M. I. Lester, *Int. Rev. Phys. Chem.*, 2020, **39**, 1-33.

46. G. Vayner, S. V. Addepalli, K. Song and W. L. Hase, *J. Chem. Phys.*, 2006, **125**.

47. L. M. M. Quijano and D. A. Singleton, *J. Am. Chem. Soc.*, 2011, **133**, 13824-13827.